Further Investigation of Acoustic Propagation Codes for Three-Dimensional Geometries

D. M. Nark *, W. R. Watson†, and M. G. Jones‡
NASA Langley Research Center

The ability to predict fan noise within complex three-dimensional aircraft engine nacelle geometries is a valuable tool in designing and assessing low-noise concepts. This work begins a systematic study to identify the areas of the design space in which propagation codes of varying fidelity may be used effectively to provide efficient design and assessment. An efficient lower-fidelity code is used in conjunction with two higher-fidelity, more computationally intensive methods to solve benchmark problems of increasing complexity. The codes represent a small sampling of the current propagation codes available or under development. Results of this initial study indicate that the lower-fidelity code provides satisfactory results for cases involving low to moderate attenuation rates, whereas, the two higher-fidelity codes perform well across the range of problems.

Nomenclature

c	sound speed, m/s
I_x	axial acoustic intensity, W/m^2
i	$\sqrt{-1}$
k, k_x	free space and axial wave number, 1/m
L_2	L2-norm of computed complex acoustic potential
M	uniform steady duct flow Mach number
m	mode number in the y-direction (short transverse duct dimension)
N	total number of grid points used in determining the error norm (L_2)
n	mode number in the z-direction (long transverse duct dimension)

Symbols:

$\beta_{m,n}$	cut-off ratio of the (m,n) mode (eqn. 2)
ζ	acoustic impedance, normalized by ρc
λ	complex modal eigenvalue, 1/m
ρ	ambient density, kg/m^3
ϕ_c, ϕ_e	computed and exact value of acoustic potential, m^2/s
φ_x	wave front propagation angle relative to the axial coordinate, deg (eqn. 3)
ψ_x	resultant propagation angle relative to the axial coordinate, deg (eqn. 4)

Abbreviations:

CDL	CDUCT-LaRC
CDL_WA	CDUCT-LaRC wide-angle
FEM3D	3D finite element
FEMQ3D	quasi-3D finite element

*Research Scientist, Research & Technology Directorate, Structural Acoustics Branch, d.m.nark@nasa.gov, Member AIAA
†Senior Research Scientist, Research & Technology Directorate, Computational Aerosciences Branch, Willie.R.Watson@nasa.gov, Senior Member AIAA
‡Senior Research Scientist, Research & Technology Directorate, Structural Acoustics Branch, michael.g.jones@nasa.gov, Senior Member AIAA

I. Introduction

THE ability to predict fan noise within complex three-dimensional aircraft engine nacelle geometries (figure 1) is a valuable tool in studying low-noise designs. Recent years have seen the development of aeroacoustic propagation codes using various levels of approximation to obtain such a capability. For instance, the propagation module of CDUCT-LaRC[1] incorporates the work of Dougherty,[2,3] which utilizes a parabolic approximation to the convected Helmholtz equation. This approach affords very efficient propagation calculations, thus allowing solutions for complex three-dimensional geometries to be handled with relatively low computational costs. This efficiency comes at the expense of reduced accuracy as the direction of propagation of an acoustic mode diverges from the preferred angle of the parabolic approximation. Additionally, loss of accuracy may occur when reflection and/or backward scattering of acoustic waves becomes important, as these effects are not captured in this formulation . Nevertheless, if appropriate care is taken to account for these limitations, CDUCT-LaRC (CDL) provides an efficient environment in which to perform three-dimensional propagation calculations. In contrast, more extensive three-dimensional codes, such as the 3D Euler solver (LEENOISE),[4] ACTRAN-AE,[5] and the Fast Scattering Code (FSC)[6] are also being developed. In addition, there has been an extension of a no-flow, 3D finite element code presented in an earlier paper[7] to include mean flow (FEM3D). Because these more extensive three dimensional codes generally offer higher fidelity at increased computational expense, it would seem appropriate to use the tools in a complementary manner. For example, the current CDUCT-LaRC propagation module could be used to identify preliminary designs and the FEM3D could then be used to refine the results. With this in mind, it is reasonable to attempt some systematic error study to identify a "working envelope" within which to use the various codes.

The focus of this work is to perform such a study by working through a series of problems incorporating increasingly complex geometries. The current version of the CDUCT-LaRC (CDL) code and the 3D finite element method (FEM3D) are considered. Results for a Quasi-3D finite element code[8] (FEMQ3D) are also compared in several cases. Although FEMQ3D is not a fully three-dimensional code, it was included to provide further confidence in solution quality and connection with previous work.[9] The other aforementioned codes were not currently included in this study due to availability and/or level of familiarity at this time. The geometries to be evaluated in the current investigation were chosen to address the possible loss of accuracy due to wide angle propagation and backward scattering from impedance discontinuities. (An investigation of the effects of reflections from internal geometries such as bifurcations, as well as the duct termination, will be provided in a future report.) Beginning with an infinite-length, hardwall rectangular duct, loss of accuracy as a function of cut-off ratio (hence, propagation angle) may be determined through comparison with analytic solutions. The inclusion of duct treatment may diminish the importance of this error, as acoustic modes tend to interact more with duct walls as they approach cut-off. Therefore, infinite-length, treated ducts will also be addressed.

As mentioned previously, problems involving backward scattering or reflections of acoustic waves are also of interest. In order to identify possible errors in calculating scattering from impedance discontinuities, the aforementioned infinite-length rectangular geometries will be used with partial acoustic treatment. Finally, the effects of reflections from internal geometries such as bifurcations, as well as from the duct termination, may also be important sources of error. It is expected that acoustic treatment will make reflections from the duct termination less important in practice. As for the effects of reflections from internal obstructions, a further study is needed.

II. Discussion

This study begins to quantify the effects of wide angle propagation on solution accuracy. The parabolic approximation assumes that acoustic waves propagate in a preferred direction. Within the CDL code, this is defined by the axial grid lines. As the true propagation angle diverges from the preferred angle, a loss of accuracy will occur. This typically manifests itself in the form of phase error, although there is also associated amplitude error. Conversely, the FEMQ3D and FEM3D codes do not incorporate a parabolic approximation and generally provide improved accuracy. In the case of the FEM3D code, this accuracy comes with increased computational expense. The FEMQ3D code, on the other hand, is limited to two-dimensional or axisymmetric geometries.

A. Hardwall Cases

The initial hardwall rectangular duct configuration was chosen to simulate the Curved Duct Test Rig (CDTR) at NASA Langley.[10] The straight duct is taken to be 0.152 m (6 in) by 0.381 m (15 in) with an overall length of 0.813 m (32 in). All calculations for the FEM3D and CDL codes were performed on computational grids of dimension 16x16x37

in the transverse, spanwise, and axial directions, respectively. Of course, this translates into a grid of dimension 16x37 for the FEMQ3D calculations. The wall-clock time (actual computation time) for the FEM3D cases was generally 2.3 minutes per case on eight 1.4 GHz Itanium 2 processors. The CDL cases were run with an average wall-clock time of 3.5 seconds on one 3.06 GHz Xeon processor, while the FEMQ3D cases ran in fractions of a second on one 1.4 GHz Itanium 2 processor. The source frequency range of 500 to 3000 Hz and flow Mach number range of 0.0 to 0.30 were also chosen to mimic CDTR test conditions. Cases including plane wave sources were selected to provide baseline error values. Higher order duct mode sources were then selected to illustrate the effects of propagation angle on solution accuracy. In all cases, the L_2-norm,

$$L_2 = \frac{1}{N}\sqrt{\sum_{i=1}^{N}(\phi_c - \phi_e)(\phi_c - \phi_e)^*} \tag{1}$$

was computed to provide an indication of global error relative to the analytically obtained exact solution. The attenuation in the duct was also calculated for comparison with analytic solutions and to provide a further measure of error for the predicted results. The attenuation is defined as the difference between the acoustic power at the exit and source planes of the duct. The acoustic power is obtained by integrating the axial intensity, I_x, over the area of the exit and entrance plane areas and taking $10\log$ of the ratio. For these case, the axial intensity is written in terms of the acoustic potential as

$$I_x = \rho c\left[k^2 M\phi\phi^* + ik\phi\phi_x^* + ikM^2\phi_x\phi^*\right]$$

which is based on the expression for acoustic intensity given by Morfey.[11]

1. Plane Wave

The capability of the FEMQ3D and CDL codes to properly handle plane wave sources was documented in initial benchmarking work.[9] Further plane wave cases were conducted to incorporate FEM3D predictions and baseline the error. The specific Mach number and source frequency for the cases considered are presented in table 1 of the Appendix. The error norm of the computed complex acoustic potential obtained from each code is also included in this table. As an alternative measure, the calculated attenuation is presented in table 2. As the attenuation should be zero in this hard wall duct, this quantity provides another indication of error. Figure 2 provides a graphical representation of the error in which the logarithm of the L_2-norm is presented as a function of frequency and Mach number. The results indicate that all codes provide reasonable results, with the FEMQ3D performing considerably better than the other codes in terms of attenuation.

2. Higher-Order Modes

In order to assess the effect of cut-off ratio (and/or propagation angle), several higher-order modal sources were considered for the hard wall geometry. The modal source information is provided in table 3. The particular combinations of Mach number, frequency, and mode number were chosen to obtain, at least in hardwall cases, a range of cut-off ratios and propagation angles. The cut-off ratio for the (m, n) mode is defined as

$$\beta_{m,n} = \frac{k}{\sqrt{1-M^2}k_x}. \tag{2}$$

Following the propagation angle definitions of Rice[12] and Farassat,[13] two angles of propagation with respect to the axial direction are computed. The propagation angle, φ_x, is based on the phase velocity and is given by

$$\cos\varphi_x = \frac{k_x}{\sqrt{k_x^2 + k_y^2 + k_z^2}} \tag{3}$$

Using the terminology of Rice, the resultant propagation angle, ψ_x, is based on the group velocity and is defined as

$$\cos\psi_x = \frac{M + \cos\varphi_x}{\sqrt{1 + M^2 + 2M\cos\varphi_x}} \tag{4}$$

The values of these quantities for the various source modes are also provided in table 3.

The L_2-norm and attenuation results are provided in tables 4 and 5. As this is again a hardwall duct, the calculated attenuation should be zero. Comparison of L_2-norm and attenuation values with those of the plane wave cases, and expected zero attenuation, indicate that all of the codes provide reasonable results. The finite element codes again display improved accuracy over the CDL code. The FEMQ3D code again stands out if the magnitude of the predicted attenuation is used as an error measure. These cases also provide some insight into the behavior of the error inherent in the parabolic approximation of the CDL code. To illustrate this further, the L_2-norm is plotted versus the cut-off ratio and two propagation angles in figures 3 through 5. As expected, the error increases as the cut-off ratio decreases (*i.e.* the mode approaches cut-off). Similarly, figures 4 and 5 show that the error increases as the angle of propagation increases. It is also interesting to note that the resultant propagation angle, ψ_x, appears to provide an improved correlation with the L_2-norm over the propagation angle, ϕ_x. This may be an important issue in attempting to curve fit the error for extension to further cases. Sample curve fits were included in the figures for illustrative purposes. Overall, the results indicate that the three codes provide satisfactory results for the hardwall cases considered. In light of this, this next step was to study cases involving acoustic treatment.

B. Full-Length Acoustic Treatment

As a first step in including the effects of acoustic treatment, the CDTR-inspired geometry of the hardwall cases was modified to include lining on one wall. In an effort to further emulate the CDTR, one 0.813 m x 0.381 m wall was taken to be treated with acoustic material having an impedance of $\zeta = 1.0 - 0.5i$. A general sketch of the set-up is presented in figure 6, with the treated wall represented by white wireframe.

1. Plane Wave

The capability of the FEMQ3D and CDL codes to handle an infinitely-lined geometry was documented in initial benchmarking work, with the results generally following expected trends.[9] The cases pursued in this work provide a wider range of propagation angles, as well as the incorporation of FEM3D results. Additionally, as in the case of the hardwall predictions, the calculations of error norm and attenuation provide the capability to further quantify the error. The Mach number and frequency range considered are provided in table 6. The eigenvalues correspond to the least-attenuated mode for n=0. The definition of cut-off ratio for treated cases is problematic, as such, this quantity is absent from the table. However, the propagation angle, ϕ_x, and resultant propagation angle, ψ_x, are retained by using the real part of the wave numbers in equations 3 and 4, as suggested by Rice.[12] A review of the L_2-norm and attenuation results in tables 7 and 8 indicate that results follow trends similar to the plane wave results. The FEMQ3D-predicted attenuation values matched the analytic code results extremely well. The FEM3D code also produces very good results, showing some expected loss of accuracy relative to the two-dimensional/axisymmetric FEMQ3D code. The CDL code also produced very good results for cases of low to moderate attenuation rate. The additional column labeled CDL_WA in these tables contains results obtained using the wide-angle correction of the parabolic approximation within the CDL propagation module. The error incurred in cases involving large attenuation rates may be connected to larger propagation angles, as evidenced by the corresponding values ϕ_x and ψ_x. The use of the wide angle correction provides some improvement (*e.g.* runs 1 and 2), coming at the expense of increased computation time. However, there appears to be some difficulty in drawing a direct connection between the CDL error and the propagation angles as computed for this treated case. For instance, the L_2-norm of the CDL results decreases for run numbers 7 through 9. Conversely, the error in predicted attenuation for run 9 is larger than that of runs 7 and 8. In light of this, some further study is needed to fully understand the possible correlation between error and propagation angles for cases in which treatment is involved.

2. Higher-Order Modes

Following the progression of source types for the hard wall cases, higher order mode sources were also considered for the treated case. The specific source information is provided in table 9. As in the previous treated case, the eigenvalues correspond to the least-attenuated mode of the given mode number, n. The error norm and attenuation predictions are also presented in tables 10 and 11. The results again show very similar trends to the previous cases, as the FEMQ3D and FEM3D codes performed very well. The CDL and CDL_WA results also compare favorably in cases of low to moderate attenuation rate. The general correlation between CDL errors and propagation angle also appears to be present, as run numbers 3, 9, and 15 show larger attenuation errors in conjunction with large propagation angles. This statement is made with some caution in light of the aforementioned anomalies, although the general trend certainly appears to be present.

C. Segmented Acoustic Treatment

As a next step in studying the effects of acoustic treatment, a duct incorporating segmented lining on one wall was considered. To mimic the CDTR geometry, hardwall sections of length 0.610 m (24 in) were added to the upstream and downstream sections of the previous full-length treated geometry. Thus, the segmented cases incorporate a straight rectangular duct of width 0.152 m (6 in) with a height of 0.381 m (15 in). The overall length of 2.032 m (80 in) is made up of three subsections: a 0.610 m (24 in) hardwall section, a 0.813 m (32 in) section with one 0.813 m x 0.381 m wall treated, and a final 0.610 m (24 in) hardwall section. A general sketch of the set-up is presented in figure 7, with the treated portion of the wall represented by white wireframe. The number of grids points in the axial direction was increased to accommodate the larger computation domain and the FEM3D and CDL codes were performed on computation grids of dimension 16x16x81 in the transverse, spanwise, and axial directions, respectively. The wall-clock time for the FEM3D cases was generally five minutes per case on eight 1.4 GHz Itanium 2 processors. The CDL cases were run with an average wall-clock time of 7.3 seconds on one 3.06 GHz Xeon processor. The main focus of these cases was to identify the effects of reflections from impedance discontinuities on the solution quality. For these initial predictions, this entailed comparing the results of the FEM3D and CDL codes to identify reflections and differences in predicted attenuation values. In order to minimize the effects of possible reflection from the duct termination, the same source and exit impedance were specified for both codes. This was achieved by performing the CDL predictions and then exporting the source and exit impedance information into the FEM3D code. This process also served as a first step in setting up the mechanism for the transfer of data between the two codes. This will ultimately allow the use of the Ffowcs Williams-Hawkings (FW-H) radiation module of CDUCT-LaRC in conjunction with the propagation results of the FEM3D code.

The source information for the upstream hardwall section was taken from the plane wave and higher-order hardwall cases of tables 1 and 3. The predicted attenuation values are provided in tables 12 and 13. As seen in previous cases, differences between the FEM3D and CDL results appear to increase as the cut-off ratio (hence, propagation angle) in the hardwall section increases. The overall attenuation values are different than the full-length treatment cases, as expected. It is also expected that cases involving larger hardwall propagation angles will entail larger reflections at the leading and trailing edges of the segmented treatment. A case in point being run number 2 of the plane wave source cases (table 12). The difference between the predicted FEM3D and CDL attenuation values are slightly larger than for the infinitely lined case. A possible cause for the slight increase may be the reflections that result from the liner discontinuity. To illustrate this point, the centerline acoustic potential amplitude and phase are presented in figures 8 and 9. A standing wave pattern is evident between the source plane and leading edge of the liner in the FEM3D results. The parabolic approximation of the CDL propagation calculations neglects these reflections and the pattern is not present in the CDL predictions. It would therefore be expected that CDL attenuation results would incur some error as the amplitude of the standing wave pattern grows. As in the case of the full-length treatment predictions however, it appears that the CDL code provides acceptable results for cases of low to moderate attenuation rate (and hence, propagation angle).

III. Concluding Remarks

As propagation codes of various levels of fidelity become available, it would seem reasonable to consider the complementary use of such codes considering the acceptable error and computational resources. This work continued such a study, focusing mainly on the 3D finite element formulation (FEM3D) of Watson[8] and the propagation module of CDUCT-LaRC.[1] The parabolic approximation of the propagation module of the CDL code was expected to show error due to wide angle propagation. CDL predictions over the range of cases considered appear to show such a trend of increasing error with increase in propagation angle (or decrease in cut-off ratio). For the hardwall cases, it appears that the resultant propagation angle, ψ_x, offers very good correlation with the L_2-norm data. However, some further understanding is necessary to completely correlate a propagation angle in the case of treated ducts. The segmented-lining cases illustrate the possible loss of accuracy due to the presence of standing wave patterns caused by back-scattering from the impedance discontinuity (generally of more importance with larger propagation angles). Generally, the CDL code produces conservative attenuation estimates, providing predictions that compare well with the FEM3D and analytic result for cases entailing low to moderate attenuation rates. The FEMQ3D and FEM3D codes compare very well with analytic results across the range of cases studied. These results support the previously proposed approach for design of low-noise concepts: use the CDL code to narrow the design space and then the FEM3D code to refine the results. Future work will incorporate further propagation codes (3-D Euler solver (LEENOISE), ACTRAN-AE, and the Fast Scattering Code) as they become available. Additionally, further insight

may be gained by extending this work to study a range of impedance values. As an end result, it is hoped that the systematic study of these aeroacoustic propagation codes will begin to define a "working envelope" within which each may be used based on acceptable errors and computation time.

References

[1]Nark, D. M., Farassat, F., Pope, D. S., and Vatsa, V., "The Development of the Ducted Fan Noise Propagation and Radiation Code CDUCT-LaRC," AIAA Paper 2003-3242, 2003.

[2]Dougherty, R. P., "A Wave-Splitting Technique for Nacelle Acoustic Propagation," AIAA Paper 97-1652, 1997.

[3]Dougherty, R. P., "A Parabolic Approximation for Flow Effects on Sound Propagation in Nonuniform, Softwall, Ducts," AIAA Paper 99-1822, 1999.

[4]Lan, J. H. and Breard, C., "Validation of 3D Acoustic Propagation Code with Analytical and Experimental Results," AIAA Paper 2005-2901, 2005.

[5]Free Field Technologies, Louvain-la-Neuve, Belgium, *MSC.ACTRAN 2005 User's Manual*, 2005.

[6]Tinetti, A. F. and Dunn, M. H., "Aeroacoustic Noise Prediction Using the Fast Scaterring Code," AIAA Paper 2005-3061, 2005.

[7]Watson, W. R., "Three-Dimensional Rectanguar Duct Code with Application to Impedance Eduction," *AIAA Journal*, Vol. 40, No. 2, 2002, pp. 217–226.

[8]Watson, W. R., Jones, M. G., and Parrott, T. L., "A Quasi-3D Theory for Impedance Eduction in Uniform Flows," AIAA Paper 2005-2848, 2005.

[9]Nark, D. M., Watson, W. R., and Jones, M. G., "An Investigation of Two Acoustic Propagation Codes for Three-Dimensional Geometries," AIAA Paper 2005-3022, 2005.

[10]C.Gerhold, Cabell, R., and Brown, M., "Development of an Experimental Rig for Investigation of Higher Order Modes in Ducts," AIAA Paper 2006-2637, 2006.

[11]Morfey, C. L., "Acoustic Energy in non-uniform flows," *Journal of Sound and Vibration*, Vol. 14, No. 2, 1971, pp. 159–170.

[12]Rice, E. J., "Modal Propagation Angles in Ducts with Soft Wall and Their Connection with Suppressor Performance," AIAA Paper 79-0624, 1979.

[13]Farassat, F. and Myers, M. K., "A Graphical Approach to Wave Propagation in a Rigid Duct," *Journal of Sound and Vibration*, Vol. 200, No. 5, 1997, pp. 729–735.

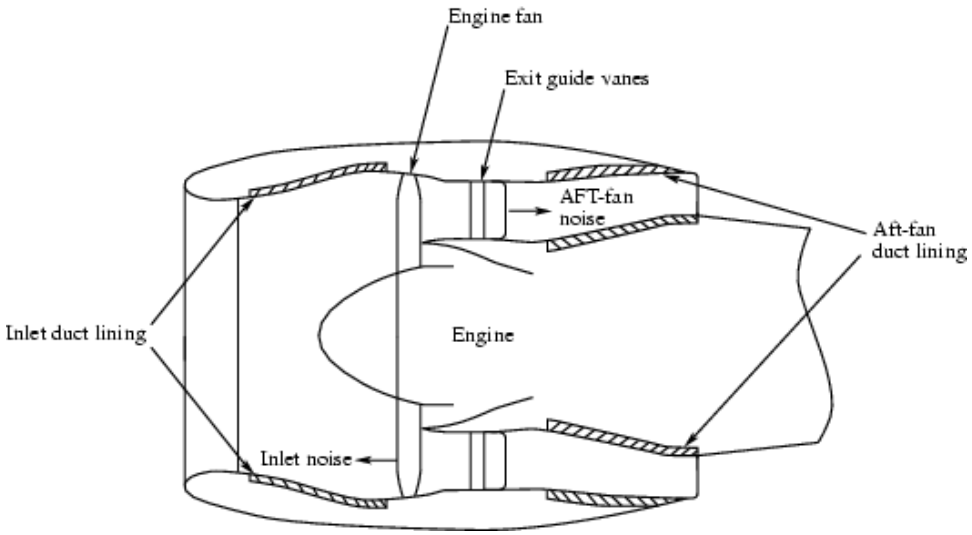

Figure 1. Typical aircraft engine with treated inlet and aft-fan ducts

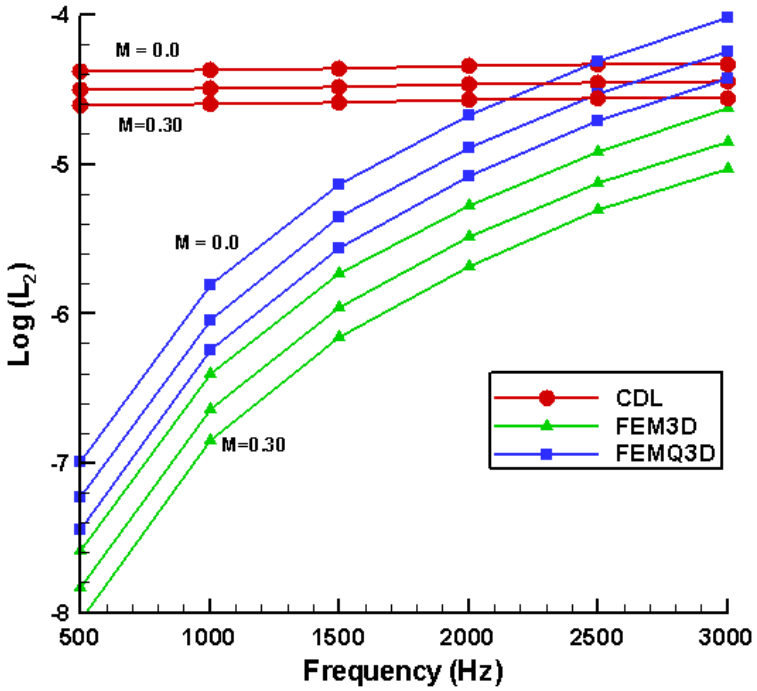

Figure 2. Logarithm of the L_2-norm for Plane-Wave Hardwall Cases

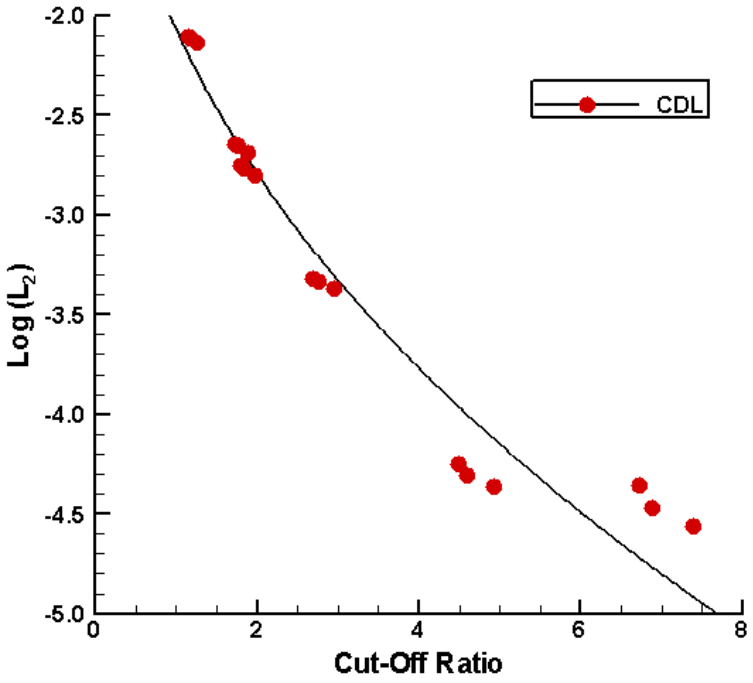

Figure 3. Logarithm of the L_2-norm Versus Cut-off Ratio, $\beta_{m,n}$ for Higher-Order Hardwall Cases

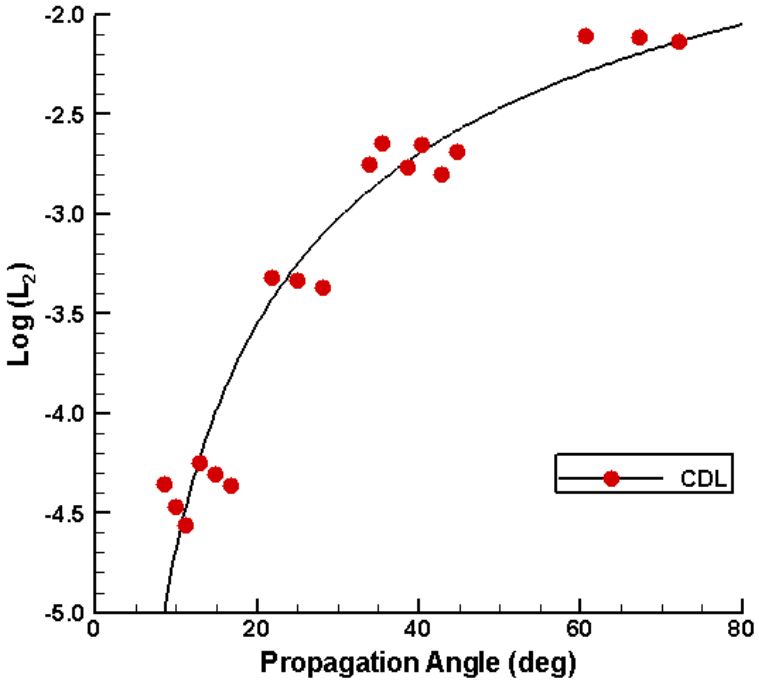

Figure 4. Logarithm of the L_2-norm Versus Propagation Angle, φ_x, for Higher-Order Hardwall Cases

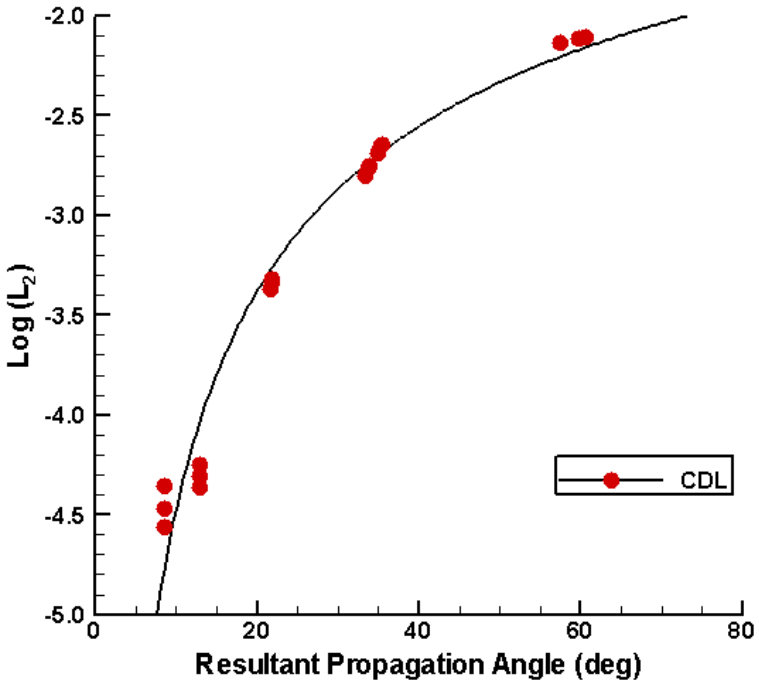

Figure 5. Logarithm of the L_2-norm Versus Resultant Propagation Angle, ψ_x, for Higher-Order Hardwall Cases

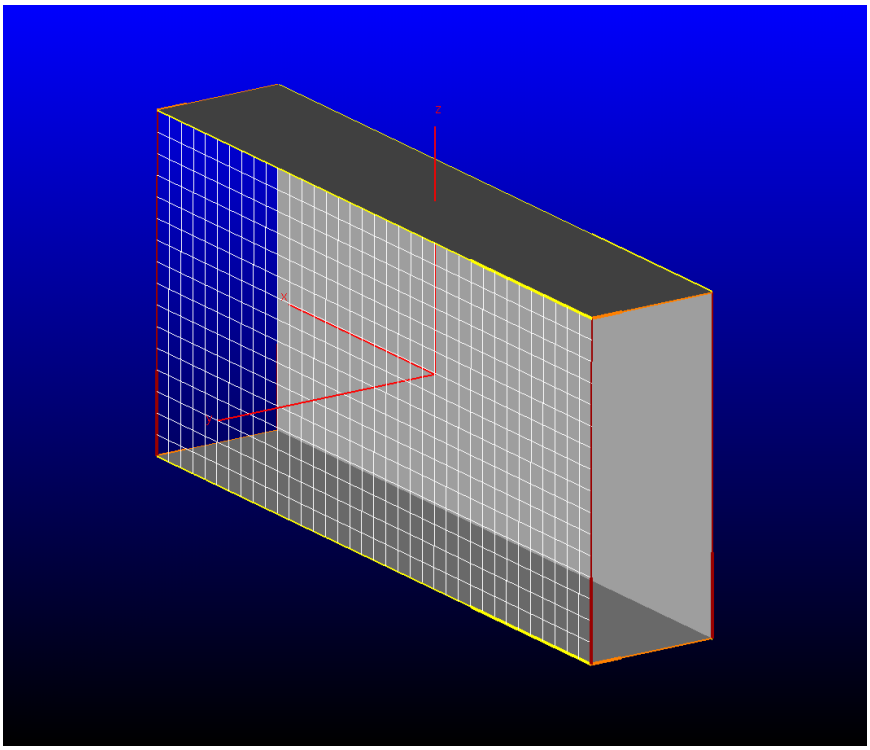

Figure 6. Baseline Geometry For Hardwall and Infinite-Treatment Cases

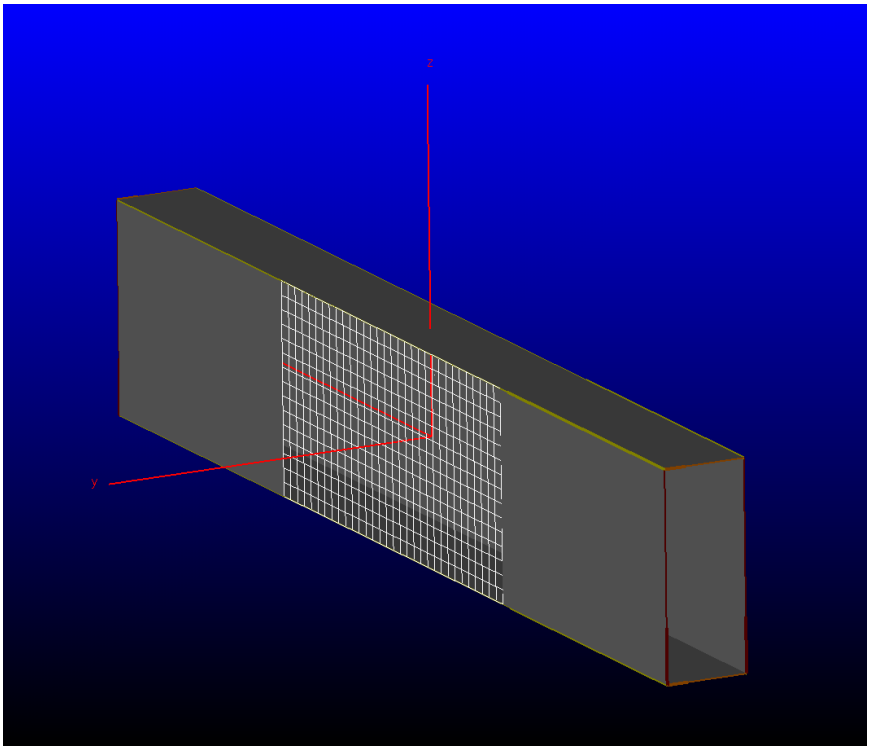

Figure 7. Baseline Geometry For Segmented-Treatment Cases

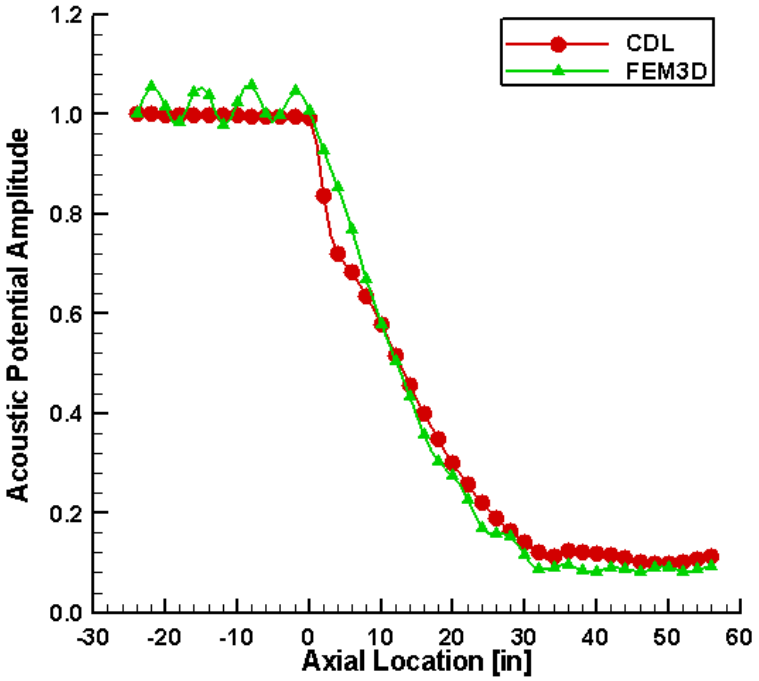

Figure 8. Comparison of Centerline Acoustic Potential Amplitude for Run 2 in Table 12

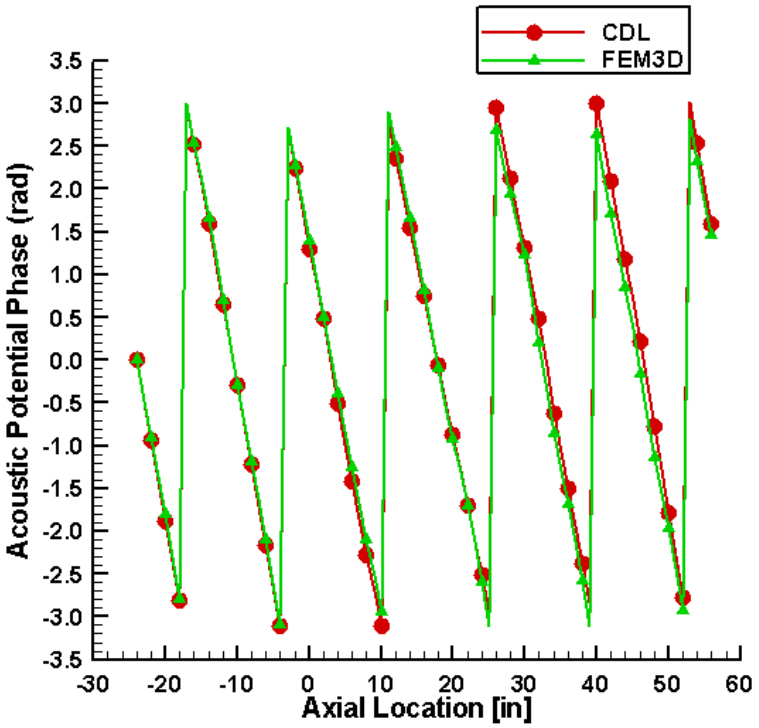

Figure 9. Comparison of Centerline Acoustic Potential Phase for Run 2 in Table 12

Tables

Run	M	Freq [Hz]	FEMQ3D	FEM3D	CDL
1	0.00	500	1.0E-7	2.6E-8	4.2E-5
2	0.00	1000	1.6E-6	3.9E-7	4.2E-5
3	0.00	1500	7.4E-6	1.8E-6	4.4E-5
4	0.00	2000	2.1E-5	5.3E-6	4.5E-5
5	0.00	2500	4.8E-5	1.2E-5	4.6E-5
6	0.00	3000	9.5E-5	2.4E-5	4.7E-6
7	0.15	500	5.9E-8	1.5E-8	3.2E-5
8	0.15	1000	9.1E-7	2.3E-7	3.2E-5
9	0.15	1500	4.4E-6	1.1E-6	3.3E-5
10	0.15	2000	1.3E-5	3.2E-6	3.4E-5
11	0.15	2500	3.0E-5	7.4E-6	3.5E-5
12	0.15	3000	5.7E-5	1.4E-5	3.6E-5
13	0.30	500	3.6E-8	9.0E-9	2.5E-5
14	0.30	1000	5.7E-7	1.4E-7	2.5E-5
15	0.30	1500	2.8E-6	6.9E-7	2.6E-5
16	0.30	2000	8.3E-6	2.1E-6	2.7E-5
17	0.30	2500	2.0E-5	4.9E-6	2.7E-5
18	0.30	3000	3.7E-5	9.4E-6	2.8E-5

Table 1. L_2Norm Results for Plane-Wave Source (Hardwall)

Run	M	Freq [Hz]	FEMQ3D	FEM3D	CDL
1	0.00	500	5.8E-15	6.9E-6	6.5E-2
2	0.00	1000	2.5E-14	9.8E-5	6.5E-2
3	0.00	1500	2.9E-15	4.0E-4	6.5E-2
4	0.00	2000	-1.9E-14	9.1E-4	6.5E-2
5	0.00	2500	1.4E-14	1.4E-3	6.5E-2
6	0.00	3000	-1.8E-14	1.2E-3	6.5E-2
7	0.15	500	-2.8E-13	2.1E-6	4.9E-2
8	0.15	1000	2.0E-10	3.0E-5	4.9E-2
9	0.15	1500	-5.3E-9	1.2E-4	4.9E-2
10	0.15	2000	2.7E-8	2.8E-4	4.9E-2
11	0.15	2500	1.1E-7	4.0E-4	4.9E-2
12	0.15	3000	-1.5E-6	2.4E-4	4.9E-2
13	0.30	500	4.6E-13	1.6E-7	3.8E-2
14	0.30	1000	-3.9E-10	1.6E-6	3.8E-2
15	0.30	1500	1.7E-8	4.7E-7	3.8E-2
16	0.30	2000	-2.1E-7	-2.9E-5	3.8E-2
17	0.30	2500	8.4E-7	-1.5E-4	3.8E-2
18	0.30	3000	-2.5E-6	-4.9E-4	3.8E-2

Table 2. Attenuation Results [dB] for Plane-Wave Source (Hardwall)

Run	M	Freq [Hz]	m	n	$\mathrm{Re}(\lambda)\left[\frac{1}{\mathrm{m}}\right]$	$\mathrm{Im}(\lambda)\left[\frac{1}{\mathrm{m}}\right]$	$\mathrm{Re}\left(\frac{k_x}{k}\right)$	$\mathrm{Im}\left(\frac{k_x}{k}\right)$	φ_x[deg]	ψ_x[deg]	β_{mn}
1	0.00	2000	0	1	0.00	0.00	0.98	0.00	12.89	12.89	4.48
2	0.00	2000	1	0	20.61	0.00	0.83	0.00	33.90	33.90	1.79
3	0.00	2000	1	3	20.61	0.00	0.49	0.00	60.60	60.60	1.15
4	0.00	3000	0	1	0.00	0.00	0.99	0.00	8.55	8.55	6.72
5	0.00	3000	1	0	20.61	0.00	0.93	0.00	21.83	21.83	2.69
6	0.00	3000	1	3	20.61	0.00	0.81	0.00	35.51	35.51	1.72
7	0.15	2000	0	1	0.00	0.00	0.84	0.00	14.80	12.88	4.59
8	0.15	2000	1	0	20.61	0.00	0.70	0.00	38.55	33.77	1.83
9	0.15	2000	1	3	20.61	0.00	0.37	0.00	67.20	59.76	1.17
10	0.15	3000	0	1	0.00	0.00	0.86	0.00	9.83	8.55	6.88
11	0.15	3000	1	0	20.61	0.00	0.80	0.00	24.99	21.79	2.75
12	0.15	3000	1	3	20.61	0.00	0.68	0.00	40.33	35.35	1.76
13	0.30	2000	0	1	0.00	0.00	0.74	0.00	16.69	12.86	4.93
14	0.30	2000	1	0	20.61	0.00	0.60	0.00	42.87	33.37	1.97
15	0.30	2000	1	3	20.61	0.00	0.28	0.00	72.10	57.45	1.26
16	0.30	3000	0	1	0.00	0.00	0.76	0.00	11.10	8.54	7.39
17	0.30	3000	1	0	20.61	0.00	0.70	0.00	28.05	21.69	2.96
18	0.30	3000	1	3	20.61	0.00	0.59	0.00	44.79	34.90	1.89

Table 3. Modal Source Information for Higher-Order Cases (Hardwall)

Run	M	Freq [Hz]	m	n	FEMQ3D	FEM3D	CDL
1	0.00	2000	0	1	1.9E-5	3.5E-6	5.7E-5
2	0.00	2000	1	0	7.8E-6	2.0E-6	1.8E-3
3	0.00	2000	1	3	1.0E-6	4.7E-7	7.8E-3
4	0.00	3000	0	1	9.1E-5	1.7E-5	4.4E-5
5	0.00	3000	1	0	5.2E-5	1.3E-5	4.8E-4
6	0.00	3000	1	3	3.2E-5	5.5E-6	2.3E-3
7	0.15	2000	0	1	1.2E-5	2.1E-6	4.9E-5
8	0.15	2000	1	0	4.2E-6	1.0E-6	1.7E-3
9	0.15	2000	1	3	3.2E-7	5.4E-7	7.7E-3
10	0.15	3000	0	1	5.4E-5	9.8E-6	3.4E-5
11	0.15	3000	1	0	3.0E-5	7.5E-6	4.6E-4
12	0.15	3000	1	3	1.8E-5	2.9E-6	2.2E-3
13	0.30	2000	0	1	7.4E-6	1.3E-6	4.3E-5
14	0.30	2000	1	0	2.3E-6	5.9E-7	1.6E-3
15	0.30	2000	1	3	1.0E-7	5.7E-7	7.3E-3
16	0.30	3000	0	1	3.5E-5	6.4E-6	2.7E-5
17	0.30	3000	1	0	1.9E-5	4.8E-6	4.3E-4
18	0.30	3000	1	3	1.0E-5	1.5E-6	2.0E-3

Table 4. L_2Norm Results for Higher-Order Mode Source (Hardwall)

Run	M	Freq [Hz]	m	n	FEMQ3D	FEM3D	CDL
1	0.00	2000	0	1	2.6E-14	8.6E-4	8.3E-2
2	0.00	2000	1	0	2.3E-13	5.5E-4	1.1E-1
3	0.00	2000	1	3	-4.3E-15	9.1E-5	1.3E-1
4	0.00	3000	0	1	-2.1E-14	1.2E-3	8.3E-2
5	0.00	3000	1	0	-1.4E-14	1.4E-3	1.1E-1
6	0.00	3000	1	3	3.9E-14	1.3E-3	1.3E-1
7	0.15	2000	0	1	-5.5E-8	2.6E-4	6.3E-2
8	0.15	2000	1	0	4.9E-9	1.2E-4	8.3E-2
9	0.15	2000	1	3	3.1E-10	1.9E-6	9.8E-2
10	0.15	3000	0	1	-1.8E-6	2.6E-4	6.3E-2
11	0.15	3000	1	0	-9.4E-7	3.0E-4	8.3E-2
12	0.15	3000	1	3	4.5E-7	2.5E-4	9.8E-2
13	0.30	2000	0	1	-3.6E-8	-3.1E-5	4.9E-2
14	0.30	2000	1	0	4.6E-8	-3.6E-5	6.5E-2
15	0.30	2000	1	3	9.2E-10	-7.7E-6	7.7E-2
16	0.30	3000	0	1	-5.4E-6	-4.7E-4	4.9E-2
17	0.30	3000	1	0	-1.7E-6	-3.6E-4	6.5E-2
18	0.30	3000	1	3	8.5E-7	-2.3E-4	7.7E-2

Table 5. Attenuation Results [dB] for Higher-Order Mode Source (Hardwall)

Run	M	Freq [Hz]	m	n	$\mathrm{Re}(\lambda)\ \left[\frac{1}{\mathrm{m}}\right]$	$\mathrm{Im}(\lambda)\ \left[\frac{1}{\mathrm{m}}\right]$	$\mathrm{Re}\left(\frac{k_x}{k}\right)$	$\mathrm{Im}\left(\frac{k_x}{k}\right)$	φ_x[deg]	ψ_x[deg]
1	0.00	500	0	0	5.52	5.74	0.71	-0.52	40.01	40.01
2	0.00	1000	0	0	9.94	5.52	0.80	-0.20	33.90	33.90
3	0.00	1500	0	0	10.99	3.18	0.88	-0.05	24.32	24.32
4	0.00	2000	0	0	10.96	2.20	0.93	-0.02	17.67	17.67
5	0.00	2500	0	0	10.87	1.69	0.96	-0.01	13.83	13.83
6	0.00	3000	0	0	10.80	1.37	0.97	0.00	11.36	11.36
7	0.15	500	0	0	4.14	5.38	0.96	-0.24	24.99	21.80
8	0.15	1000	0	0	7.92	6.61	0.85	-0.16	26.66	23.26
9	0.15	1500	0	0	10.83	4.66	0.81	-0.07	25.80	22.51
10	0.15	2000	0	0	11.03	3.09	0.83	-0.03	19.83	17.28
11	0.15	2500	0	0	10.98	2.33	0.84	-0.01	15.76	13.72
12	0.15	3000	0	0	10.91	1.88	0.85	-0.01	13.03	11.34
13	0.30	500	0	0	3.24	4.86	0.86	-0.17	22.30	17.21
14	0.30	1000	0	0	6.14	6.52	0.78	-0.12	23.02	17.76
15	0.30	1500	0	0	9.45	6.46	0.74	-0.08	24.71	19.08
16	0.30	2000	0	0	10.97	4.33	0.73	-0.04	22.08	17.04
17	0.30	2500	0	0	11.05	3.15	0.74	-0.02	17.85	13.76
18	0.30	3000	0	0	11.01	2.5	0.75	-0.01	14.82	11.42

Table 6. Modal Information for Plane-Wave Source (Full-Length Treatment)

Run	M	Freq [Hz]	m	n	FEMQ3D	FEM3D	CDL	CDL_WA
1	0.00	500	0	0	6.4E-8	1.6E-8	1.0E-3	1.1E-3
2	0.00	1000	0	0	4.7E-7	1.2E-7	4.6E-4	2.7E-4
3	0.00	1500	0	0	5.1E-6	1.3E-6	3.4E-4	2.2E-4
4	0.00	2000	0	0	2.8E-5	7.1E-6	1.3E-4	9.1E-5
5	0.00	2500	0	0	9.5E-5	2.4E-5	7.6E-5	7.3E-5
6	0.00	3000	0	0	2.5E-4	6.2E-5	6.7E-5	6.8E-5
7	0.15	500	0	0	5.6E-8	1.4E-8	9.2E-4	9.5E-4
8	0.15	1000	0	0	3.4E-7	8.4E-8	4.6E-4	4.2E-4
9	0.15	1500	0	0	1.9E-6	4.8E-7	2.9E-4	1.9E-4
10	0.15	2000	0	0	1.1E-5	2.8E-6	1.3E-4	9.7E-5
11	0.15	2500	0	0	4.1E-5	1.0E-5	8.7E-5	8.5E-5
12	0.15	3000	0	0	1.1E-4	2.7E-5	7.8E-5	7.7E-5
13	0.30	500	0	0	2.3E-8	5.8E-9	8.9E-4	9.0E-4
14	0.30	1000	0	0	2.7E-7	6.7E-8	5.6E-4	5.4E-4
15	0.30	1500	0	0	1.0E-6	2.5E-7	3.5E-4	3.3E-4
16	0.30	2000	0	0	4.9E-6	1.2E-6	1.4E-4	1.4E-4
17	0.30	2500	0	0	1.8E-5	4.6E-6	1.0E-4	1.1E-4
18	0.30	3000	0	0	5.0E-5	1.3E-5	9.0E-5	9.0E-5

Table 7. L_2Norm Results for Plane-Wave Source (Full-Length Treatment)

Run	M	Freq [Hz]	m	n	FEMQ3D	FEM3D	CDL	CDL_WA	Analytic
1	0.00	500	0	0	22.57	21.95	19.96	21.78	22.57
2	0.00	1000	0	0	22.99	22.35	20.92	21.47	22.98
3	0.00	1500	0	0	9.62	9.35	8.3	9.03	9.61
4	0.00	2000	0	0	4.81	4.68	4.54	4.79	4.81
5	0.00	2500	0	0	2.89	2.81	2.85	2.96	2.89
6	0.00	3000	0	0	1.93	1.87	1.94	1.99	1.92
7	0.15	500	0	0	15.62	15.19	15.10	16.13	15.62
8	0.15	1000	0	0	20.33	19.76	19.98	19.46	20.33
9	0.15	1500	0	0	13.69	13.31	12.32	13.05	13.69
10	0.15	2000	0	0	6.78	6.59	6.48	6.83	6.78
11	0.15	2500	0	0	4.02	3.91	3.96	4.11	4.02
12	0.15	3000	0	0	2.66	2.59	2.66	2.72	2.66
13	0.30	500	0	0	11.17	10.86	11.76	12.33	11.17
14	0.30	1000	0	0	15.12	14.96	15.59	15.30	15.11
15	0.30	1500	0	0	15.97	15.53	14.63	14.61	15.97
16	0.30	2000	0	0	9.39	9.13	9.04	9.41	9.39
17	0.30	2500	0	0	5.46	5.31	5.40	5.59	5.46
18	0.30	3000	0	0	3.57	3.47	3.56	3.65	3.57

Table 8. Attenuation Results [dB] for Plane-Wave Source (Full-Length Treatment)

Run	M	Freq [Hz]	n	$\mathrm{Re}(\lambda)\ \left[\frac{1}{\mathrm{m}}\right]$	$\mathrm{Im}(\lambda)\ \left[\frac{1}{\mathrm{m}}\right]$	$\mathrm{Re}\left(\frac{k_x}{k}\right)$	$\mathrm{Im}\left(\frac{k_x}{k}\right)$	φ_x[deg]	ψ_x[deg]
1	0.00	2000	0	10.96	2.20	0.96	-1.8E-2	17.21	17.21
2	0.00	2000	1	10.96	2.20	0.93	-1.9E-2	21.73	21.73
3	0.00	2000	3	10.96	2.20	0.68	-2.6E-2	46.93	46.93
4	0.00	3000	0	10.80	1.37	0.98	-4.9E-3	11.23	11.23
5	0.00	3000	1	10.80	1.37	0.97	-5.0E-3	14.19	14.19
6	0.00	3000	3	10.80	1.37	0.87	-5.5E-3	29.13	29.13
7	0.15	2000	0	11.03	3.09	0.83	-2.6E-2	19.83	17.28
8	0.15	2000	1	11.04	3.05	0.80	-2.6E-2	24.94	21.75
9	0.15	2000	3	11.03	2.74	0.56	-3.2E-2	52.80	46.55
10	0.15	3000	0	10.91	1.88	0.85	-6.8E-3	13.03	11.34
11	0.15	3000	1	10.91	1.87	0.84	-6.8E-3	16.38	14.26
12	0.15	3000	3	10.90	1.80	0.74	-7.3E-3	33.26	29.08
13	0.30	2000	0	10.97	4.33	0.73	-3.6E-2	22.08	17.04
14	0.30	2000	1	11.01	4.19	0.71	-3.6E-2	27.82	21.51
15	0.30	2000	3	11.10	3.23	0.46	-3.6E-2	57.83	45.48
16	0.30	3000	0	11.01	2.50	0.75	-9.1E-3	14.82	11.42
17	0.30	3000	1	11.00	2.48	0.74	-9.1E-3	18.55	14.30
18	0.30	3000	3	10.98	2.26	0.64	-9.1E-3	37.17	28.85

Table 9. Modal Source Information for Least-Attenuated Modes (Full-Length Treatment)

Run	M	Freq [Hz]	n	FEMQ3D	FEM3D	CDL	CDL_WA
1	0.00	2000	0	2.8E-5	7.1E-6	1.34E-4	9.1E-5
2	0.00	2000	1	2.6E-5	4.6E-6	1.7E-4	9.6E-5
3	0.00	2000	3	7.4E-6	1.0E-6	2.6E-3	1.3E-3
4	0.00	3000	0	2.5E-4	6.2E-5	6.7E-5	6.8E-5
5	0.00	3000	1	2.4E-4	4.3E-5	7.7E-5	6.0E-5
6	0.00	3000	3	1.6E-4	2.7E-5	8.6E-4	3.0E-4
7	0.15	2000	0	1.1E-5	2.8E-6	1.3E-4	9.7E-5
8	0.15	2000	1	1.0E-5	1.8E-6	1.6E-4	9.2E-5
9	0.15	2000	3	2.6E-6	6.4E-7	2.3E-3	1.1E-3
10	0.15	3000	0	1.1E-4	2.7E-5	7.8E-5	7.7E-5
11	0.15	3000	1	1.0E-4	1.9E-5	8.4E-5	6.7E-5
12	0.15	3000	3	6.8E-5	1.1E-5	8.0E-4	2.7E-4
13	0.30	2000	0	4.9E-6	1.2E-6	1.4E-4	1.4E-4
14	0.30	2000	1	4.4E-6	7.9E-7	1.5E-4	1.2E-4
15	0.30	2000	3	9.5E-7	6.0E-7	1.9E-3	8.8E-4
16	0.30	3000	0	5.0E-5	1.3E-5	9.0E-5	9.0E-5
17	0.30	3000	1	4.9E-5	8.9E-6	8.9E-5	7.5E-5
18	0.30	3000	3	3.2E-5	5.1E-6	7.1E-4	2.2E-4

Table 10. L_2Norm Results for Higher-Order Modes Source (Full-Length Treatment)

Run	M	Freq [Hz]	n	FEMQ3D	FEM3D	CDL	CDL_WA	Analytic
1	0.00	2000	0	4.81	4.68	4.54	4.79	4.81
2	0.00	2000	1	4.95	4.81	4.48	4.74	4.95
3	0.00	2000	3	6.73	6.54	4.48	4.72	6.73
4	0.00	3000	0	1.93	1.87	1.94	1.99	1.92
5	0.00	3000	1	1.95	1.89	1.93	1.98	1.95
6	0.00	3000	3	2.16	2.10	1.93	1.97	2.16
7	0.15	2000	0	6.78	6.59	6.48	6.83	6.78
8	0.15	2000	1	6.89	6.70	6.35	6.71	6.88
9	0.15	2000	3	8.31	8.08	6.15	6.49	8.31
10	0.15	3000	0	2.66	2.59	2.66	2.72	2.66
11	0.15	3000	1	2.68	2.60	2.62	2.69	2.68
12	0.15	3000	3	2.85	2.77	2.59	2.66	2.85
13	0.30	2000	0	9.39	9.13	9.04	9.41	9.39
14	0.30	2000	1	9.36	9.10	8.78	9.19	9.35
15	0.30	2000	3	9.51	9.25	8.05	8.49	9.51
16	0.30	3000	0	3.57	3.47	3.56	3.65	3.57
17	0.30	3000	1	3.57	3.47	3.50	3.59	3.57
18	0.30	3000	3	3.57	3.47	3.39	3.48	3.57

Table 11. Attenuation Results [dB] for Higher-Order Modes Source (Full-Length Treatment)

Run	M	Freq [Hz]	FEM3D	CDL
1	0.00	500	22.06	20.17
2	0.00	1000	21.42	18.73
3	0.00	1500	8.54	8.34
4	0.00	2000	5.28	5.18
5	0.00	2500	3.67	3.79
6	0.00	3000	2.8	2.93
7	0.15	500	15.37	15.17
8	0.15	1000	19.14	18.76
9	0.15	1500	10.76	10.34
10	0.15	2000	6.35	6.21
11	0.15	2500	4.13	4.37
12	0.15	3000	3.18	3.36
13	0.30	500	11.09	11.79
14	0.30	1000	14.49	14.81
15	0.30	1500	11.99	11.55
16	0.30	2000	7.19	7.04
17	0.30	2500	5.01	4.87
18	0.30	3000	3.73	3.75

Table 12. Attenuation Results [dB] for Plane-Wave Source (Segmented Treatment)

Run	M	Freq [Hz]	m	n	FEM3D	CDL
1	0.00	2000	0	1	5.46	5.16
2	0.00	2000	1	0	9.63	9.40
3	0.00	2000	1	3	10.32	9.24
4	0.00	3000	0	1	2.94	2.94
5	0.00	3000	1	0	8.27	7.87
6	0.00	3000	1	3	8.59	7.88
7	0.15	2000	0	1	6.67	6.14
8	0.15	2000	1	0	10.60	10.20
9	0.15	2000	1	3	12.27	10.04
10	0.15	3000	0	1	3.27	3.35
11	0.15	3000	1	0	8.02	8.18
12	0.15	3000	1	3	8.45	8.21
13	0.30	2000	0	1	7.30	6.97
14	0.30	2000	1	0	11.10	10.88
15	0.30	2000	1	3	11.26	10.76
16	0.30	3000	0	1	3.80	3.73
17	0.30	3000	1	0	8.28	8.20
18	0.30	3000	1	3	8.65	8.24

Table 13. Attenuation Results [dB] for Higher-Order Mode Source (Segmented Treatment)